JOURNAL OF GUIDANCE, CONTROL, AND DYNAMICS
Vol. 30, No. 5, September–October 2007

Survey of Theory and Steering Laws of Single-Gimbal Control Moment Gyros

Haruhisa Kurokawa
National Institute of Advanced Industrial Science and Technology, Tsukuba, Ibaraki 305-8564 Japan

DOI: 10.2514/1.27316

A geometric theory regarding singularity problems of single gimbal control moment gyrosystems is outlined. Most control moment gyrosystems have impassable and inescapable singular states that obstruct continuous changes of the total angular momentum vector. The remaining problem of the theory regarding degenerate singularity is described with an unproved conjecture. Based on the theory, various steering laws such as gradient methods and singularity robust methods for the pyramid-type control moment gyrosystem, and those for variable speed control moment gyros are surveyed and analyzed. Problems of the attitude control by these steering laws are examined by geometrical analyses without numerical simulation.

Nomenclature

$\boldsymbol{C}$	=	Jacobian matrix
$\boldsymbol{c}_i$	=	torque direction vector of the ith CMG unit
$\hat{\boldsymbol{c}}$	=	unit eigenvector in $\boldsymbol{H}$ space
$\boldsymbol{g}_i$	=	gimbal direction vector of the ith CMG unit
$\boldsymbol{H}$	=	total angular momentum vector of the system
$\boldsymbol{h}_i$	=	normalized angular momentum vector of the ith CMG unit
n	=	number of CMG units in the system
p_i	=	$1/q_i$
Q	=	quadratic form at a singular state
q_i	=	$\boldsymbol{u} \cdot \boldsymbol{h}_i$
$\boldsymbol{T}$	=	output torque vector of the system
t	=	time
$\boldsymbol{u}$	=	singular vector, unit normal to all $\boldsymbol{c}_i$ at a singular state
ε_i	=	sign at a singular state
κ	=	Gaussian curvature of a singular surface
λ_j	=	singular value of the matrix $\boldsymbol{C}$
σ	=	$(\sigma_1, \ldots, \sigma_n)$, a CMG state
σ_i	=	gimbal angle of the ith CMG unit
ϕ_i	=	orthonormal basis in tangent space of σ space
ω	=	gimbal rate vector obtained by a steering law

Superscripts

N	=	null vector
S	=	vector at a singular state
T	=	torque producing vector
t	=	transpose of vector and matrix

I. Introduction

A SINGLE-GIMBAL control moment gyro (CMG) system is regarded as an effective torque generator for attitude control both for large space stations and small agile satellites because of its large torque amplification capability. Three or more single-gimbal CMG units are necessary for three-axis attitude control. A steering law gives each unit's motion, usually each unit's gimbal rate, to generate a required torque, which is provided by an attitude controller. Using an appropriate steering law, the CMG system is expected to make a rapid change of its angular momentum vector to reach its maximum for maneuvering and to make a precise control of torque for pointing and tracking. Singularity is the most serious problem for these tasks. The possible output torque does not cover the 3-D space at a singular state. Points on the border of the range of the angular momentum vector are trivially singular. Other than those, any CMG system has singular states, which form surfaces inside the border, and such singular states must be avoided. Various singularity avoidance methods have been studied.

The pseudoinverse solution has been tried as an exact method for steering law calculation [1]; additional null solutions were used for singularity avoidance using a gradient method [2–4]. Even with various objective functions as singularity measures, such gradient methods were insufficiently successful, especially for the pyramid-type (four-skew) system. Then, varieties of singularity robust (SR) inverse methods were proposed, which attempted singularity avoidance by allowing torque error [5–9]. Recently, variable-speed CMGs (VSCMG), which were once studied as integrated power and attitude control devices [10], have been revived for their singularity avoidance capability [11–15].

Mathematical studies of CMG singularity are essential for design and evaluation of a steering law, as well as for selection and evaluation of system configurations. The work by Margulies and Aubrun [16], which has offered a general theory, has remained the

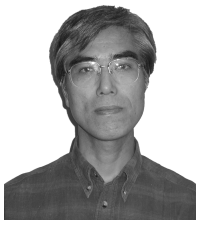

Haruhisa Kurokawa received B.E. and M.E. degrees in precision machinery engineering, and a Dr. Eng. degree in aeronautics and astronautics from the University of Tokyo, respectively, in 1978, 1981, and 1997. He currently heads the Distributed System Design Research Group, Intelligent Systems Research Institute, National Institute of Advanced Industrial Science and Technology (AIST), Japan. His main research subjects are kinematics of mechanisms, distributed autonomous systems, and nonlinear control. His current research theme is a modular robotic system.

Received 15 August 2006; accepted for publication 6 March 2007.

most important and most referred paper. In contrast, works by Tokar published originally in Russian have been virtually ignored, even though they were published during the same year as [16] and presented various theoretical ideas and calculation results [17–20]. About ten years were spent to catch up to the results presented by Tokar through studies following the paper by Margulies and Aubrun [21–27]. Some confusion still remains in relation to the theory regarding terminology and interpretations; for this reason, theoretical studies have not been used effectively for analyses and evaluation of recent steering law studies.

This paper is intended as a survey and analysis of steering laws based on the theory of CMG singularities. After a summary of basic terms and equations in Sec. II, the various research streams of theory will be briefly surveyed. Because theory itself is a basis of steering law analyses, a general and unified theory will be outlined after this survey. A remaining problem regarding a degenerate state will be formulated.

Section IV presents a survey of steering laws. Because all steering laws have been analyzed and evaluated using simulations and experiments in their original papers, geometric analyses and qualitative evaluations of those steering laws' motions are provided in Sec. V. Section VI gives a guide for future studies. Mathematical details and remaining problems are briefly explained in the Appendix.

II. Basic Mathematics

Variables and equations, most of which are based on [16], are defined in this section. The same notation as those in [16] are used to the greatest extent possible, although most expressions are produced using vector algebra. Satellite dynamics and the effects of gimbal acceleration are not considered unless stated otherwise.

A. General Description

A general system, especially a 3-D redundant system, is considered consisting of n (>3) single-gimbal CMG units. The angular momentum of all CMG units is set to unity. The system state is defined by the set of all gimbal angles, each of which is denoted by σ_i for $i = 1, \ldots, n$. No limits are assigned to the angles.

Three mutually orthogonal unit vectors for each CMG unit are defined as a gimbal vector $\boldsymbol{g}_i$, an angular momentum vector $\boldsymbol{h}_i$, and a torque vector $\boldsymbol{c}_i$, where

$$\boldsymbol{c}_i = \partial \boldsymbol{h}_i / \partial \sigma_i = \boldsymbol{g}_i \times \boldsymbol{h}_i \tag{1}$$

The gimbal vectors are fixed and the others are dependent upon the gimbal angles. In this paper, the same symbol is used to represent a vector in the Euclidean space as well as its representation in a column vector based on the CMG system's coordinate basis.

The system configuration is defined by the arrangement of the $\boldsymbol{g}_i$. Many configurations have been investigated, most of which are categorized as follows:

1) Independent-type configuration: all $\boldsymbol{g}_i$ are different and no three of them are coplanar.

2) Coplanar configuration: all $\boldsymbol{g}_i$ are on the same plane.

3) Multiparallel type configuration: $\boldsymbol{g}_i$ are grouped sharing the same directions.

As examples, a pyramid (four-skew) configuration is of the first category and a roof-type (two-speed) configuration belongs to the latter two.

The total angular momentum $\boldsymbol{H}$ and the output torque $\boldsymbol{T}$ are given by

$$\boldsymbol{H} = \boldsymbol{H}(\sigma) = \sum_{i=1}^{n} \boldsymbol{h}_i \tag{2}$$

$$\boldsymbol{T} = -\sum_i \boldsymbol{c}_i \, d\sigma_i/dt = -\boldsymbol{C}\, d\sigma/dt \tag{3}$$

where σ is the state variable, $\sigma = (\sigma_1, \ldots, \sigma_n)$, and $d\sigma/dt = (d\sigma_1/dt, \ldots, d\sigma_n/dt)^t$ is an n-dimensional column vector. The $3 \times n$ matrix $\boldsymbol{C}$ is the Jacobian of Eq. (2). Hereafter, σ and $\boldsymbol{H}$ are, respectively, called a state and a point.

B. Steering Law

A steering law obtains the gimbal rates, $\boldsymbol{\omega} = (\omega_1, \ldots, \omega_n)^t$, with which the resulting torque in Eq. (3) is equal to the torque command $\boldsymbol{T}_{\text{com}}$. For $n > 3$, the general solution is given as

$$\omega = -\boldsymbol{C}^t (\boldsymbol{C}\boldsymbol{C}^t)^{-1} \boldsymbol{T}_{\text{com}} + \omega^N \tag{4}$$

The first term in the right is the Moor–Penrose pseudoinverse solution, which gives the minimal norm solution. The second term, ω^N, is a solution of the homogeneous equation as $\boldsymbol{C}\omega^N = (0, 0, 0)^t$; it is called a *null vector*. (The term *null motion* is used as a finite change of the state, keeping $\boldsymbol{H}$ the same.)

It is noteworthy that two kinds of torque are not shown in Eqs. (3) and (4), which must be included in the precise equation of the attitude control problem. One is the reaction torque by acceleration of gimbal rotation. It is usually ignored for steering laws in practice, as described in Sec. V.A. The other is the gyro-effect torque caused by the vehicle's rotation. This torque is usually included in the dynamics equation of the attitude control system; consequently, it is not ignored but included in $\boldsymbol{T}_{\text{com}}$ in Eq. (4).

C. Singular State and Surface

When the system is singular, that is, $\det(\boldsymbol{C}\boldsymbol{C}^t) = 0$, all torque vectors $\boldsymbol{c}_i$ become coplanar and the possible outputs $\boldsymbol{T}$ of Eq. (3) do not span 3-D space. The rank of $\boldsymbol{C}$ can become one if all $\boldsymbol{g}_i$ are on the same plane, as is true of a coplanar system. Hereinafter, an independent-type configuration is assumed. For that reason, the rank does not reduce to one.

All singular $\boldsymbol{H}$ as points in 3-D space form a continuous and mostly smooth surface called a *singular surface*. It includes the *angular momentum envelope* (the *envelope* for short) and an internal singular surface. The singular surface and its corresponding σ are calculable using the methods described in [16,26].

Let all variables at a singular state be superscripted by S. At a singular state σ^S, a unit vector $\boldsymbol{u}$ normal to all $\boldsymbol{c}_i^S$ along with related variables are defined as

$$\boldsymbol{u} \cdot \boldsymbol{c}_i^S = 0 \tag{5}$$

$$q_i = \boldsymbol{u} \cdot \boldsymbol{h}_i^S \tag{6}$$

$$p_i = 1/q_i \tag{7}$$

$$\varepsilon_i = \begin{cases} +, & q_i > 0 \\ 0, & q_i = 0 \\ -, & q_i < 0 \end{cases} \tag{8}$$

These equations do not uniquely define the variables, because there are two choices of $\boldsymbol{u}$. Though unique definition is not necessary for geometric analysis, a condition is assumed hereafter for simpler explanation in the next section so that the number of positive ε_i is not less than that of negative ones. Also see the footnote in Sec III.C.

The Gaussian curvature κ of the singular surface is described as

$$1/\kappa = 1/2 \sum_i \sum_j p_i p_j [\, \boldsymbol{c}_i^S \quad \boldsymbol{c}_j^S \quad \boldsymbol{u} \,]^2 \tag{9}$$

where $[\, \boldsymbol{a} \quad \boldsymbol{b} \quad \boldsymbol{c} \,]$ is a box product of three vectors such that $[\, \boldsymbol{a} \quad \boldsymbol{b} \quad \boldsymbol{c} \,] = \boldsymbol{a} \cdot (\boldsymbol{b} \times \boldsymbol{c})$ [16,28].

It is noteworthy that the range of $\boldsymbol{H}$ is assumed to be simply connected for any configuration without a hole or a tunnel. This is not trivial and has not been proved yet [16] (see Appendix). The

Gaussian curvature and the principal curvatures have an important meaning, as described later, but other properties of the surface described by differential geometric tools have not been related clearly to singularity analysis and steering laws. For such mathematics, [24,26] provide good explanations.

D. Singular Value Decomposition

The matrix $\boldsymbol{C}$ can be represented using its singular values λ_i and unitary transformations $\boldsymbol{U}$ and $\boldsymbol{V}$, as follows:

$$\boldsymbol{C} = \boldsymbol{U}\begin{bmatrix} \lambda_1 & 0 & 0 & 0 & & 0 \\ 0 & \lambda_2 & 0 & 0 & \dots & 0 \\ 0 & 0 & \lambda_3 & 0 & & 0 \end{bmatrix}\boldsymbol{V}^t \tag{10}$$

Throughout this paper, the following is assumed:

$$\lambda_1 \geq \lambda_2 \geq \lambda_3 \geq 0 \tag{11}$$

At a nonsingular state, $\lambda_3 \neq 0$ and the unitary matrices $\boldsymbol{U}$ and $\boldsymbol{V}$ can be constructed by

$$\begin{aligned} \boldsymbol{U} &= [\,\hat{\boldsymbol{c}}_1 \quad \hat{\boldsymbol{c}}_2 \quad \hat{\boldsymbol{c}}_3\,], \\ \boldsymbol{V} &= [\,\varphi_1^T \quad \varphi_2^T \quad \varphi_3^T \quad \varphi_1^N \quad \varphi_2^N \quad \dots \quad \varphi_{n-3}^N\,] \end{aligned} \tag{12}$$

where three $\hat{\boldsymbol{c}}_i$ are the eigenvectors corresponding to the singular values λ_i and which make up an orthonormal basis in the Euclidean space, and all φ_i make up a corresponding orthonormal basis of the tangent space of σ. The three φ_i^T $(i = 1, 2, 3)$ are Moor–Penrose pseudoinverse solutions, and φ_i^N $(i = 1, \dots, n-3)$ are null vectors in Eq. (4).

At a singular state, the minimal singular value λ_3 becomes 0 and the two matrices in Eq. (12) become

$$\boldsymbol{U} = [\,\hat{\boldsymbol{c}}_1^T \quad \hat{\boldsymbol{c}}_2^T \quad \boldsymbol{u}\,], \qquad \boldsymbol{V} = [\,\varphi_1^T \quad \varphi_2^T \quad \varphi_1^N \quad \varphi_2^N \quad \dots \quad \varphi_{n-2}^N\,] \tag{13}$$

III. Theory of Singular Surface

The intended goal of the theory was first to obtain the size and shape of the workspace of a CMG system for selection of a configuration. Margulies and Aubrun established a general method described in Sec. II.C, as well as a general formulation of a steering law and null vectors [16]. They introduced a quadratic form, which this author followed to formulate a classification of a singular state according to whether it is escapable by a null motion [21]. Bedrossian et al. [24] and Wie [26] pursued a more detailed investigation of the differential geometric properties of a singular surface related to escapability.

During the same year as the work by Margulies and Aubrun, Tokar presented an impassable singularity theory based on the same quadratic form and evaluated various configurations [17–20]. Because the original paper of those were in Russian and their English translations used different terminology, such as a "gyrostabilizer" or a "gyrodyne" for a CMG, those works did not become well-known in the West. Nearly ten years were spent by the aforementioned researchers to match Tokar's results.

Two terms, impassability and escapability, were used independently for similar properties of a singular state. In the following, their definitions and the theory of CMG singularity will be summarized. Remaining problems regarding a degenerate state, which [24,26] emphasized as important for escapability analysis, will be formulated.

A. Quadratic Form, Passability, and Escapability

In [16], a quadratic form $Q(d\sigma)$ at a singular state is defined as a second-order infinitesimal change of $\boldsymbol{H}$ along the $-\boldsymbol{u}$ direction by an infinitesimal displacement $d\sigma$ (see Appendix):

$$Q(d\sigma) = -2(\boldsymbol{u} \cdot \Delta \boldsymbol{H}) = \sum q_i (d\sigma_i)^2 \tag{14}$$

An infinitesimal displacement $d\sigma$ is an element of the n-dimensional tangent space of the σ space. Three special subspaces exist: the null space, its complementary space, and the singularly constrained space. (An expression of bases of the three spaces is shown in [23].) The null space $\{d\sigma^N\}$ is $n-2$-dimensional and spanned by $\{\varphi_i^N\}$ in Eq. (13); its complementary space $\{d\sigma^T\}$ is 2-D and spanned by $\{\varphi_i^T\}$. The singularly constrained space is 2-D and its element, $d\sigma^S$, keeps the system singular. Two spaces of $d\sigma^N$ and $d\sigma^T$ are sufficient to cover the whole $d\sigma$ space, but two spaces of $d\sigma^N$ and $d\sigma^S$ are not always so. For the explanations in this section, we presume the following property at a singular state:

Surface Regularity: The singular surface is regular, that is, smooth, at $\boldsymbol{H}^S$, which implies that $\mathrm{d}\boldsymbol{H}(d\sigma^S)$ span the surface, and that $d\sigma^S$ and $d\sigma^N$ are independent, and that they all span n-dimensional space.

This condition is assumed in [16] without any discussion. Actually, this holds at most singular states for an independent-type configuration (see Sec. III.D).

By this condition, any $d\sigma$ and the corresponding $Q(d\sigma)$ are decomposable as [25,28]

$$d\sigma = d\sigma^S + d\sigma^N \tag{15}$$

$$Q(d\sigma) = Q(d\sigma^S) + Q(d\sigma^N) \tag{16}$$

* The first term of the right-hand side in Eq. (16), $Q(d\sigma^S)$, is the second fundamental form of the singular surface (see Appendix). See [16] for another expression.

The last term of Eq. (16), $Q(d\sigma^N)$, gives *passability* of the singular surface as follows: Because the first term on the right is attributable to the curved singular surface, the last term represents second-order infinitesimal displacement of $\boldsymbol{H}$ to $-\boldsymbol{u}$ direction from the singular surface. If this quadratic form is definite, that is, if it is the same sign for any $d\sigma^N$, any motion is restricted to the same side of the surface in $\boldsymbol{H}$ space. Because the quadratic form and its derivatives are continuous with respect to σ^S, $\boldsymbol{H}^S$ of definite form make up a certain area of the surface, through which it is not possible to pass from one side to the other if σ is in the (infinitesimal) neighborhood of corresponding singular states. In this sense, such an area of the surface with a definite form is termed *impassable* [20]. Similarly, an area of the surface with an indefinite form is *passable*.

Another aspect of this form category is *escapability* [21,24,26]. There exist directions in the $d\sigma^N$ space (null space), along which the quadratic form is zero if a singular state is passable (i.e., hyperbolic) having an indefinite $Q(d\sigma^N)$. As the motion by $d\sigma^N$ keeps $\boldsymbol{H}$ on the singular surface and $d\sigma^N$ is independent from $d\sigma^S$ under surface regularity condition, escape from a passable singular state on a regular surface is always possible. In contrast, no escape is possible at an elliptic (i.e., impassable) singular state.

Therefore, passability and escapability are compatible where the surface is regular. Although other terms such as "elliptic/hyperbolic" [16,21,24,26] and "definite/indefinite" [22,23] have also been used; the terms "impassable/passable" are used in this paper because they were defined earliest.

B. Passability and Surface Curvature

A relation is apparent between passability and the local shape of a singular surface. The signature of $Q(d\sigma)$ is the sum of the signatures of the two quadratic forms $Q(d\sigma^S)$ and $Q(d\sigma^N)$ by Sylvester's law of inertia. Because the signature of $Q(d\sigma)$ is $\{\varepsilon_i\}$ and that of $Q(d\sigma^S)$ includes signs of two principal curvatures, there can be only three impassable surface types [23].

Type 1: If all ε_i are positive, $Q(d\sigma^N)$ is always positive definite. The $\boldsymbol{H}$ of this type is on the envelope and the Gaussian curvature is positive; consequently, the surface is convex to $\boldsymbol{u}$.

*It is helpful to represent $d\sigma^S$ and $d\sigma^N$, respectively, as column vectors $d\theta^S \in R^2$ and $d\theta^N \in R^{n-2}$ based on the orthonormal basis of the two subspaces. The two quadratic forms are expressed as $d\theta^{St} Q^S d\theta^S$ and $d\theta^{Nt} Q^N d\theta^N$, where Q^S and Q^N are 2×2 and $(n-2) \times (n-2)$ matrices.

Type 2: If all ε_i but one are positive and the Gaussian curvature is negative, $Q(d\sigma^N)$ is positive definite. Part of this type surface is on the envelope, but the remaining part is internal. The surface is curved as a hyperbolic saddle surface.

Type 3: If all ε_i but two are positive and the signature of the first quadratic form is $(-,-)$, $Q(d\sigma^N)$ is positive definite. The surface of this type is fully internal and is concave to $\boldsymbol{u}$, and its Gaussian curvature κ is positive. Note that a positive κ does not always imply impassability because the signature of $Q(d\sigma^S)$ can be $(+,+)$ with positive κ.[†]

The preceding explanation ignores the case in which $\boldsymbol{u}$ is parallel to $\mathbf{g}_i$, that is, $\varepsilon_i = q_i = 0$. Equations (15) and (16) hold even in this case, and one signature of $Q(d\sigma^S)$ is 0, hence $\kappa = 0$. Therefore, the signature of $Q(d\sigma^N)$ does not contain 0 and a similar discussion is possible.

C. Impassable Surface Example

Based on this classification method and by various methods in [16], impassable surface regions are calculable. Any independent-type configuration has an internal impassable surface that is distinct from the envelope because a type 2 surface extends smoothly inside from the envelope. The symmetric six-unit system has only type 2 internal surfaces very near its envelope [20]. However, systems with $n = 4$ or 5 have both type 2 and type 3 surfaces extending far inside. For the symmetric pyramid configuration in Fig. 1, impassable surface patches are obtained as in Fig. 2. (A similar figure is shown in [20].) Impassable surfaces appear similar to connected strips forming a parallelepiped. A continuous curved line with analytical expressions is obtained to represent this framework of surface strips [25]. Edges of the strip are shaped as folds; they are borders of impassable and passable regions (see a cross section in Fig. 3a). On the folding border, $1/\kappa$ in Eq. (9) is 0, and surface regularity does not hold. Figure 2a is a part of the internal impassable surfaces. All are obtained by successive $1/4$ rotations about the Z axis based on the system's symmetry (Fig. 2b).

As for multiparallel type configurations, some differences exist in analysis, as described next. However, impassable surfaces of such systems are also defined by $Q(d\sigma^N)$ and can be calculated. Impassable surfaces of the roof-type system are the point at the origin and two unit circles [22]. Unlike independent-type configurations, there are systems with no internal impassable surface with $n \geq 6$.[‡]

D. Regularity Condition and Degenerate State

For the examinations in Secs. III.A and III.B, an independent type of configuration and surface regularity are assumed. Although passability and escapability are definable for any configuration, we require additional analysis for exceptional cases. Moreover, if the regularity condition does not hold, that is, one $d\sigma^S$ direction becomes included in the null space, and if a finite null motion along this $d\sigma^S$ maintains singularity, escape by this null motion is not possible. Bedrossian et al. [24] discussed this problem and termed this state a degenerate state. A degenerate state is a special case in which surface regularity breaks.

Examples of degenerate states that have been identified are all 2-D systems and multiparallel-type configurations [24]. Singularity and surface geometry of 2-D systems and multiparallel-type configurations differ from those of independent-type configurations. For example, a singular surface corresponding to $\boldsymbol{u}$ parallel to $\boldsymbol{g}_i$ is a unit circle for an independent-type configuration, but it is a circular plate for a multiparallel-type configuration. Moreover, 2-D systems with

[†]If $n = 4$ and the total signature is $(-,-,+,+)$, the surface with signature $(++)$ is also impassable and positive κ is the sufficient condition for type 3. In this case, it is better for consistent definition to redefine $\boldsymbol{u}$ by $-\boldsymbol{u}$ and ε by $-\varepsilon$ so that $\boldsymbol{u}$ represents the direction in which $\boldsymbol{H}$ motion is impossible.

[‡]The proofs of passability of multiparallel type configurations in [23,28] were based on surface curvature, irrespective of surface regularity; hence they are not correct. An identical conclusion, however, is obtained by direct evaluation of $Q(d\sigma^N)$. For example, a six-unit system as a pair of three-unit planar systems has no internal impassable surface because each planar subsystem has no internal impassable state as a 2-D system.

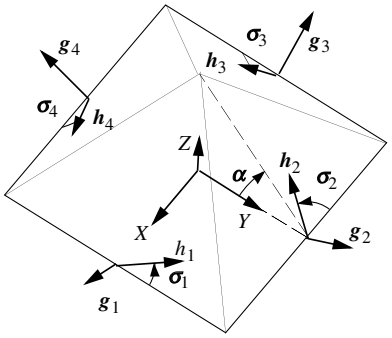

Fig. 1 Symmetric pyramid-type system. The pyramid is half of a regular hexahedron for $\cos^2\alpha = 1/3$.

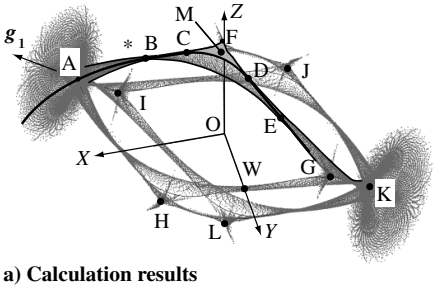

a) Calculation results

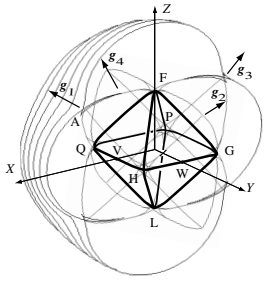

b) Total impassable surface structure

Fig. 2 Impassable surface of the symmetric pyramid-type system. a) Impassable singular points are calculated with $\boldsymbol{\varepsilon} = (-,+,+,+)$ and $(-,-,+,+)$ for various u scattered on the Gaussian sphere. There is an analytical expression along line ABCDE. The surface patches around AB and inside BCDEB are of type 2, and that inside CFDC is of type 3. The cross section near * is shown in Fig. 3a. b) All lines symmetrically transformed from the curved line ABCDE are shown with a half-cut envelope.

$n \geq 3$ and most multiparallel type systems with $n \geq 6$ have no internal impassable state.

For an independent-type system, surface regularity breaks on the borderline of an impassable surface and a passable surface. Through calculations, no degenerate state has been found for various independent-type configurations. This engenders the conjecture 1 in the Appendix that no degenerate state exists for an independent-type configuration. Because most multiparallel type systems have no problem of impassability, it is expected that degenerate states cause a problem only for the roof-type system. To construct a comprehensive theory, these must be proved in a future study (see Appendix).

E. Inverse Manifold and Topological Analysis

Passability is defined using infinitesimal analysis; it remains unclear how far the effect of an impassable surface extends. Inverse manifolds and their change clearly show the meaning of impassability and expected $\boldsymbol{H}$ deviation to avoid singularity [25,27]. Through consideration of the topological connection of manifolds, a global problem of the pyramid-type system was found.

1. Inverse Manifold

A steering law is a method to obtain gimbal rates that correspond to a given torque command: the change of $\boldsymbol{H}$. A system's behavior can

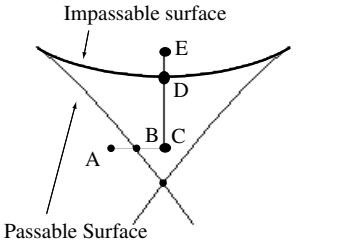

a) Singular surface cross section

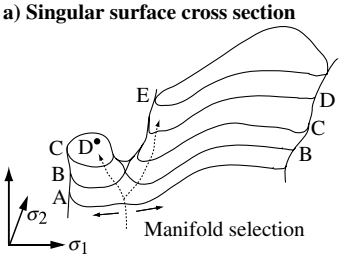

b) Change of manifold

Fig. 3 Path of H and change of inverse manifold. Manifolds are obtained by computer calculations and illustrated in 2-D space.

be viewed by a path of σ that corresponds to a path of $\boldsymbol{H}$ if time is ignored. All possible paths of σ are visible by inverse images of the mapping of Eq. (2).

The inverse image is a set of subspaces that are mutually disjoint. Each subspace is either an $n-3$-dimensional manifold or a similar complex, which is hereafter termed a *null-motion manifold* or a *manifold* for short. The shapes of manifolds in the neighborhood of a singular state are characterized by setting the quadratic form $Q(d\sigma^N)$ constant. It resembles either a superellipsoid or a superhyperbolic surface. The number of disjoint manifolds is held constant when $\boldsymbol{H}$ moves without encountering a singular surface.

Figure 3a shows part of a cross section of the singular surface of the symmetric pyramid-type system in Fig. 1. A manifold is topologically a loop in the 4-D torus space. Along with the $\boldsymbol{H}$ motion described by ABCDE, the manifold bifurcates at B, and one of them terminates at D (Fig. 3b). Once the system state is on such a terminating manifold in the triangular region, there is no way to reach the other manifold by any null motion other than driving $\boldsymbol{H}$ out of the region through a passable surface.

This example illustrates the effect of an impassable surface covering a region surrounded by singular surfaces. The shape and the size of an impassable surface are important for evaluation of possible error in the $\boldsymbol{H}$ path.

2. Global Problem

Topological theory does not allow one-to-one continuous mappings from $\boldsymbol{H}$ to σ over the range of $\boldsymbol{H}$ [29]. This fact is not always a problem for a steering law. If an $\boldsymbol{H}$ workspace without an impassable surface is considered, a gradient method works effectively. In this case, a discontinuous and one-to-multi mapping gives local maxima of the objective function for a gradient method. The question is the size of such workspace. A workspace without an impassable surface can be almost equal to the envelope in the case of the symmetric six unit system, but it must be reduced greatly in the case of the pyramid-type system.

Apparently, the problem of impassability is not sufficiently serious to exclude all impassable surfaces from the workspace when viewed with the aforementioned manifolds. Local avoidance of the impassable singularity shown in Fig. 3b seems possible if an appropriate manifold is selected before entering the triangular region [27]. However, if a reduced $\boldsymbol{H}$ workspace shown in Fig. 4 is considered, the aforementioned possibility was eliminated first by simulation results [30], and subsequently by geometrical analysis [25]. This problem, hereafter called a global problem, holds that no steering law for the symmetric pyramid-type system can continue to exactly generate arbitrary torque inside the workspace shown in Fig. 4.

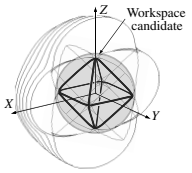

Fig. 4 Spherical workspace candidate. The sphere entirely surrounds a hexahedral frame structure made of impassable surface strips.

IV. Survey of Steering Laws

Various steering laws have been proposed in the literature. Although most steering laws were formulated for a general system, the symmetric pyramid configuration is mainly assumed in the following unless stated otherwise. Steering laws are grouped as exact methods, offline planning, an SR inverse family, and methods for variable-speed CMGs.

A. Steering Law by Exact Solution

1. Moor–Penrose Pseudoinverse Steering Law

The pseudoinverse solution, which is the first term on the right in Eq. (4), is orthogonal to the tangent space of the null-motion manifold. It has often been claimed that this method tends to drive the system to approach a singular state [3]. There is actually no such tendency to approach or to escape from a singular state from a continuous control perspective because the motion of σ by the pseudoinverse solution remains on a curve that is normal to the manifolds. Discrete time control, however, induces the system to approach a passable state as follows: The shapes of manifolds near a passable singular state are hyperbolic; consequently, their normal curves are also hyperbolic and convex to the singular state. Stepwise change of σ_i moves the system state away from the normal curve and nearer to the singular state.

2. Gradient Method

Various proposed steering laws with singularity avoidance are categorized as gradient methods [2–4]. They use the solution of Eq. (4); a null motion is determined to increase (or decrease) an objective function, which represents distance (or similarity) to singular states such as $\det(\boldsymbol{C}\boldsymbol{C}^t)$, the minimum eigenvalue of $\boldsymbol{C}$, or the condition number of $\boldsymbol{C}$. Any passable singular state is avoidable and escapable by any such method, and no impassable one is escapable. Therefore, this method is effective for systems such as three double-gimbal CMGs or multiparallel type systems that have no internal impassable singularity. On the other hand, because of the global problem, no exact type steering law including a gradient method is effective for systems with a few CMG units, such as the pyramid-type system and the roof-type system.

3. Steering Laws for the Roof-Type System

Studies of the roof-type CMG system were made more than 15 years ago [31,32]. Those steering laws were based on decomposition of $\boldsymbol{H}$ into planar subsystems. Because singularity problems were better clarified for the roof-type system, those steering laws were designed to avoid most of the internal singular states through the use of exact methods. The remaining singular states were not escapable [31], or were avoided using a discontinuous motion [32].

4. Preferred Angle Setting and Constrained Steering Law

After simulation results by Bauer [30] indicating the global problem, Vadali et al. proposed preferred gimbal angles to assure singularity avoidance for command torque in a specified direction [33]. Such a method can be effective either for maneuvering or for pointing under the condition that the disturbance torque is roughly estimated along a certain direction. Even for maneuvering, its problem is that it is not always able to reach the preferred angles by null motion. For pointing, even when disturbance torque is in a certain direction, the CMG system controlled by a usual steering law,

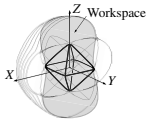

Fig. 5 Restricted workspace for constrained steering law.

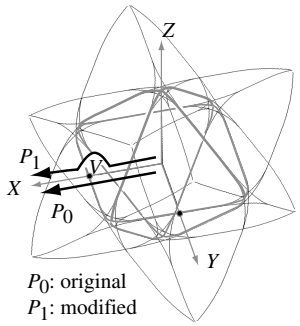

Fig. 6 Offline reshaping of H path.

such as a gradient method, does not always return to the same preferred angles when $\boldsymbol{H}$ moves around and back to the initial $\boldsymbol{H}$.

The constrained steering law solved these problems for the pyramid configuration [34]. It uses one-to-one mapping from $\boldsymbol{H}$ to σ inside a restricted workspace shown in Fig. 5, which is set as almost maximum under the limitation by the global problem. Because of its one-to-one mapping nature, it requires no method of singularity avoidance, but it does require an additional process to keep $\boldsymbol{H}$ inside a predefined workspace. Discontinuous change is necessary to switch between the three selections of workspaces. This method resembles the method in [32] for the roof-type system.

B. Offline Planning Approach

Obtaining a continuous σ path for a given path of $\boldsymbol{H}$ is possible in most cases. An offline planning method by Paradisso seeks an optimal σ path combining near-exact solutions by the SR inverse method in the next section [35]. This method, however, necessitates brute force calculation and is therefore time-consuming, even using the theory described in the preceding section.

Two more realistic planning methods exist. Figure 6 shows that the easiest way for the pyramid configuration is offline reshaping of the $\boldsymbol{H}$ path to avoid an impassable surface. Because the entire impassable surface can be roughly modeled as a set of parallelepipeds, such reshaping requires little calculation. The most effective but rather time-consuming way is to plan and optimize maneuvering with the full satellite's dynamics model, including the CMG system [36].

C. Steering Law Allowing Torque Error

After failure by gradient methods that are intended at singularity avoidance in σ space, other methods were tried: they avoid the singularity in $\boldsymbol{H}$ space and allow error in output torque. They are based on quadratic optimization of similar functions; they are listed in this section and analyzed in Sec. V.

1. *Singular Pseudoinverse Steering Law (SPI)*

At a singular state, there is no solution of Eq. (3), except when the desired $\boldsymbol{T}$ is orthogonal to the vector $\boldsymbol{u}$. Even when an exact solution exists, the solution is not obtained using the pseudoinverse solution in Eq. (4) because of mathematical singularity. A candidate solution was proposed such that it gives the minimal norm solution if $\boldsymbol{T}_{\text{com}}$ is orthogonal to $\boldsymbol{u}$; otherwise the output error is minimized so that the resulting $\boldsymbol{T}$ is equal to the projection of $\boldsymbol{T}_{\text{com}}$ onto the plane orthogonal to $\boldsymbol{u}$. The formulation of this in [16] can be written as

$$\omega = -\boldsymbol{C}^t(\boldsymbol{C}\boldsymbol{C}^t + \boldsymbol{u}\boldsymbol{u}^t)^{-1}\boldsymbol{T}_{\text{com}} \tag{17}$$

by presuming an additional CMG unit whose torque vector, $\boldsymbol{c}_{n+1}$, equals $\boldsymbol{u}$. Another expression using singular value decomposition in Eqs. (11) and (15) is made as

$$\omega = -[\,\varphi_1^T \quad \varphi_2^T\,]\begin{bmatrix} 1/\lambda_1 & 0 \\ 0 & 1/\lambda_2 \end{bmatrix}[\,\hat{\boldsymbol{c}}_1^T \quad \hat{\boldsymbol{c}}_2^T\,]^t\boldsymbol{T}_{\text{com}} \tag{18}$$

2. *Singularity Robust Inverse Steering Law (SRI)*

The method called the singularity robust (SR) inverse steering law is an extension of the preceding method, but it is applicable even to a nonsingular state. Nakamura and Hanafusa proposed this for the control of a robot manipulator [37], then Bedrossian et al. applied it to CMG control [5]. This method minimizes the weighted sum of squared norm $|\omega|^2$, and the square of the output torque error. The solution is given as

$$\omega = -\boldsymbol{C}^t(\boldsymbol{C}\boldsymbol{C}^t + k\boldsymbol{I})^{-1}\boldsymbol{T}_{\text{com}} \tag{19}$$

where $\boldsymbol{I}$ is an $n \times n$ unit matrix and k is a positive parameter. Another expression is

$$\omega = -[\,\varphi_1^T \quad \varphi_2^T \quad \varphi_3^T\,] \times \begin{bmatrix} \lambda_1/(\lambda_1^2+k) & 0 & 0 \\ 0 & \lambda_2/(\lambda_2^2+k) & 0 \\ 0 & 0 & \lambda_3/(\lambda_3^2+k) \end{bmatrix} \times [\,\hat{\boldsymbol{c}}_1 \quad \hat{\boldsymbol{c}}_2 \quad \hat{\boldsymbol{c}}_3\,]^t\boldsymbol{T}_{\text{com}} \tag{20}$$

3. *Singular Direction Avoidance Steering Law (SDA)*

The solution by the preceding SRI at a singular state for $\boldsymbol{T}_{\text{com}}$ orthogonal to $\boldsymbol{u}$ differs from the true solution given by SPI. Ford and Hall proposed a method to correct this problem as follows [7]:

$$\omega = -[\,\varphi_1^T \quad \varphi_2^T \quad \varphi_3^T\,] \times \begin{bmatrix} 1/\lambda_1 & 0 & 0 \\ 0 & 1/\lambda_2 & 0 \\ 0 & 0 & \lambda_3/(\lambda_3^2+k) \end{bmatrix}[\,\hat{\boldsymbol{c}}_1 \quad \hat{\boldsymbol{c}}_2 \quad \hat{\boldsymbol{c}}_3\,]^t\boldsymbol{T}_{\text{com}} \tag{21}$$

Because $\hat{\boldsymbol{c}}_3$ approaches $\boldsymbol{u}$ as the state approaches singularity, and because the first two diagonal terms, $1/\lambda_1$ and $1/\lambda_2$, are the same as in Eq. (18), this is a smoother extension of SPI than SRI. Another expression corresponding to Eq. (17) is

$$\omega = -\boldsymbol{C}^t(\boldsymbol{C}\boldsymbol{C}^t + k\hat{\boldsymbol{c}}_3\hat{\boldsymbol{c}}_3^t)^{-1}\boldsymbol{T}_{\text{com}} \tag{22}$$

4. *Perturbed SR Inverse Steering Law (PSR)*

All the preceding methods give $\omega = 0$ for $\boldsymbol{T}_{\text{com}}$ parallel to $\boldsymbol{u}$ at a singular state; therefore, escape from the singular state is not possible. Oh and Vadali proposed a method using perturbation to prevent $\boldsymbol{T}_{\text{com}}$ from becoming parallel to $\boldsymbol{u}$ near a singular state [6]. Wie et al. proposed a similar method [8]:

$$\omega = -\boldsymbol{C}^t(\boldsymbol{C}\boldsymbol{C}^t + k\boldsymbol{A})^{-1}\boldsymbol{T}_{\text{com}} \tag{23}$$

Therein, the 3×3 matrix $\boldsymbol{A}$ is given as

$$\boldsymbol{A} = \begin{bmatrix} 1 & \varepsilon_3 & \varepsilon_2 \\ \varepsilon_3 & 1 & \varepsilon_1 \\ \varepsilon_2 & \varepsilon_1 & 1 \end{bmatrix} \tag{24}$$

with three small periodic dither functions ε_i.

5. *Off-Diagonal SR Inverse Steering Law (o-DSR)*

Using any method, saturation singularity is unavoidable. From a singular state, when the direction of $\boldsymbol{T}_{\text{com}}$ is toward $\boldsymbol{u}$, the system should leave the singular surface. None of the methods described previously, however, can yield a solution. Wie et al. proposed a method as an extension to the preceding PSR to solve this problem, as [9]

$$\omega = -\boldsymbol{W}\boldsymbol{C}^t(\boldsymbol{C}\boldsymbol{W}\boldsymbol{C}^t + k\boldsymbol{A})^{-1}\boldsymbol{T}_{\text{com}} \tag{25}$$

where $\boldsymbol{A}$ is the same matrix as Eq. (24) and the matrix $\boldsymbol{W}$ is nearly diagonal with small value α as

$$\boldsymbol{W} = \begin{bmatrix} W_1 & \alpha & \alpha & \alpha \\ \alpha & W_2 & \alpha & \alpha \\ \alpha & \alpha & W_3 & \alpha \\ \alpha & \alpha & \alpha & W_4 \end{bmatrix} > 0 \tag{26}$$

D. Variable-Speed CMG

A variable-speed CMG (VSCMG) system was studied as an integrated power and attitude control system (IPACS) [10]; it has been revived recently [11–15]. It is a combination of a usual CMG system and a reaction wheel (RW) system, both having capability of torque generation. Because the torque by the RW subsystem is usually far smaller than that by the CMG subsystem, using the CMG subsystem is more effective for attitude control. The singularity avoidance of the CMG subsystem, therefore, is always necessary. The RW subsystem is useful for singularity avoidance of the CMG subsystem; gradient methods were proposed in [12,14].

V. Analysis of Steering Law

For most studies, evaluations of steering laws have been made using numerical simulations that include satellite dynamics. However, it is not easy to analyze and evaluate CMG motions merely using simulations. Moreover, most of studies address only maneuvering. In the following, a CMG motion alone will be considered first to evaluate steering laws. Then simplified motions will be analyzed considering a satellite's dynamic behavior.

A. Acceleration term

Oh and Vadali [6] and Ford and Hall [7] introduced an acceleration term of gimbal angles into Eq. (3) and produced steering laws and simulations. Because the acceleration torque of a CMG is usually far smaller than the gyro-effect torque [38], and because this term has only a transient effect that slightly changes the $\boldsymbol{H}$ path, including this term in a steering law has little effect on singularity avoidance, but it is worthwhile for an exact dynamical simulation.

B. CMG Motion by SR Inverse-Type Steering Law

The theory of a singular surface presented in Sec. III provides explanations of the SR inverse-type steering laws: how they work, why escape from singularity is assured, and how large the error is [28].

The CMG motion solved using the preceding methods, SPI, SR, SDA, PSR, and o-DSR, is understood geometrically as follows: The SPI drives $\boldsymbol{H}$ along the singular surface, according to its definition. All methods including SPI are based on minimization of similar quadratic functions; most have similar expressions by singular value decomposition. Therefore, all methods make point $\boldsymbol{H}$ follow and slide along the singular surface. This *sliding* of $\boldsymbol{H}$ is conceptualized as a particle pushed by a force against an elastic wall.

The differences among the methods are illustrated in Fig. 7. The eigenvector $\hat{\boldsymbol{c}}_3$, which corresponds to the minimal singular value, is almost parallel to $\boldsymbol{u}$ at the singular state when the system is near a singular state. The other two eigenvectors, $\hat{\boldsymbol{c}}_1$ and $\hat{\boldsymbol{c}}_2$, are on a plane, denoted as TP in Fig. 7, almost parallel to the tangent plane to the singular surface. The SPI generates a torque along the tangent plane according to its definition. Similarly, the output torque by SDA, $\boldsymbol{T}_{\text{SDA}}$, has a component ($\boldsymbol{T}_1$) on TP which is a projection of $\boldsymbol{T}_{\text{com}}$ to TP. Its component to $\hat{\boldsymbol{c}}_3$ is made smaller than that of $\boldsymbol{T}_{\text{com}}$. Because the singular values are measures of $|\boldsymbol{T}|/|\boldsymbol{\omega}|$, the component on the plane TP, $\boldsymbol{T}_2$, of the output torque, $\boldsymbol{T}_{\text{SR}}$, by SRI, PSR or o-DSR deviates slightly to the $\hat{\boldsymbol{c}}_1$ direction from $\boldsymbol{T}_1$ and is shortened by the term including k (Fig. 7).

A passable singularity is always avoidable through proper use of a null vector if a gradient method is combined. Sliding by an SR inverse-type steering law, therefore, occurs mostly near an impassable surface. (The discussion requires slight modification because the passable surface might also affect the CMG motion near the border of impassable and passable surfaces.) According to the fact described in Sec. III.C, the case in Fig. 8a as a gimbal-lock situation occurs only when approaching a type 1 surface: the envelope. For an internal impassable surface of type 2 or type 3, there is always a direction in which the surface is curved with negative curvature to $\boldsymbol{u}$. Therefore, possible behaviors are like those shown in Figs. 8b and 8c; it is always possible by sliding to navigate along and escape from the impassable surface as long as the command direction is almost fixed.

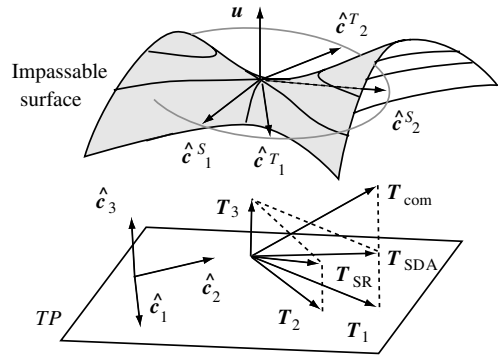

Fig. 7 Generated torque by SR inverse-type steering laws. Vectors, $\hat{c}^S_j$, as principal directions of the surface do not always coincide with $\hat{c}^T_j$.

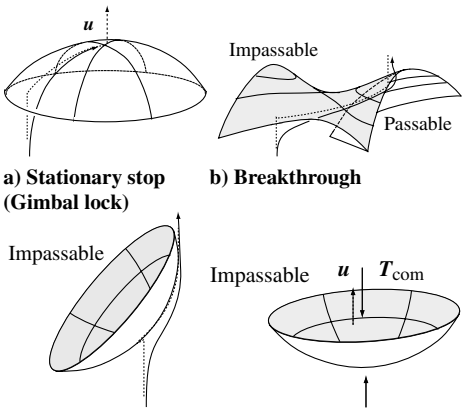

Fig. 8 Behaviors by a sliding motion along a singular surface.

The solution by SPI, SDA, and SRI becomes 0 and the system does not move like a dead lock or a gimbal lock when $\boldsymbol{T}_{\text{com}}$ is parallel to $\boldsymbol{u}$ (Fig. 8d). This dead lock, however, is an unstable equilibrium because the singular surface has negative curvature. Sliding will start and continue until the system escapes from the surface if some dither or an error causes the system move. The PSR realizes this dithering.

Deviation of the $\boldsymbol{H}$ path by this sliding motion can be estimated using singular surface geometry because of the discussion in Sec. III.E. In case of the pyramid-type system, the type 2 impassable surface near points B and E in Fig. 2a resembles a narrow strip with negative curvature to the narrow direction. Therefore, sliding motion and possible error of $\boldsymbol{H}$ before escaping from this surface are roughly estimated by the strip width. On the other hand, the type 3 surface near point M in Fig. 2a is wider and it is curved by negative curvature to every direction. The direction of sliding motion and deviation of $\boldsymbol{H}$ might vary according to torque command and steering laws. Although the actual output torque by each method varies, deviation of $\boldsymbol{H}$, as a time integral of the torque error, is dependent mostly on the singular surface geometry.

C. Escape from Saturation Singularity and Computation

The method to escape from a singular state that the o-DSR offers can be explained theoretically. Any $d\sigma^S$ produces motion staying on a singular surface and a null vector $d\sigma^N$ makes second-order

infinitesimal motion away from the surface, as described in the preceding section. A null vector therefore induces the system to move from the singular surface, as clarified by considering the following reverse process: The eigenvector φ_3^T induces the system to approach the singular surface, and when the system reaches the surface, this eigenvector φ_3^T becomes a null vector. Among all null vectors, the eigenvector for the maximum eigenvalue of the quadratic form $Q(d\sigma^N)$ gives the fastest escape from the surface. All SR methods render the component of the output torque to both $\pm\boldsymbol{u}$ directions as small. In fact, this is not necessary when $\boldsymbol{H}$ is receding from the singular surface, that is, when $(\boldsymbol{T}_{\rm com} \cdot \boldsymbol{u}) > 0$, and the exact solution is useful.

How does o-DSR use a null vector? The matrix $\boldsymbol{A}$ in Eq. (24) is the unit matrix and the matrix $\boldsymbol{W}$ in Eq. (26) is diagonal if perturbation (dither) terms are ignored. The SR inverse solution by Eq. (19) minimizes the quadratic function as

$$|\boldsymbol{T}_{\rm com} - \boldsymbol{C}\omega|^2 + |\omega|^2 \tag{27}$$

The solution of this is in the space of φ^T. Because the spaces of φ^T and φ^S are not always identical, this solution by itself has a component of a null vector in the decomposition of Eq. (15). Because the o-DSR uses a modified function,

$$|\boldsymbol{T}_{\rm com} - \boldsymbol{C}\omega|^2 + \omega^t \boldsymbol{W}\omega \tag{28}$$

the solution might not be in the space of φ^T and includes a null vector if diagonal elements of $\boldsymbol{W}$ are not identical. Consequently, o-DSR can use a null vector to leave a singular surface.

With respect to calculation, useful methods are outlined in [16]. The vector $\boldsymbol{u}$ is only defined at a singular state, but this vector as well as $\hat{\boldsymbol{c}}_3$ near a singular state can be approximated as $\boldsymbol{c}_i \times \boldsymbol{c}_j$ having maximum norm. Null vectors are obtainable considering a virtual CMG unit whose $\boldsymbol{c}$ is $\boldsymbol{u}$ (or $\hat{\boldsymbol{c}}_3$) and using a method described in [16]. Therefore, calculation of eigenvectors is not always necessary for use of the methods described earlier.

D. Singularity Avoidance of VSCMG

A VSCMG system has no singularity except saturation. Any singular state of the CMG subsystem is therefore escapable if the RW effect is considered. Singularity avoidance using the proposed methods [12,14] can be analyzed geometrically using a simple example as follows:

Using additional variables Ω_i as flywheel speeds, all expressions in the preceding sections are changed by multiplying vectors $\boldsymbol{c}_i$ and $\boldsymbol{h}_i$ by Ω_i. Considering the case in which all $\Omega_i = 1$ and the CMG subsystem's state is near the impassable singular state of $\sigma = (-\pi/2, \pi, \pi/2, \pi)$, as in Fig. 9a. This singular state corresponds to point V in Fig. 2b. Three approaches can be used to move away from this singular state, without altering total $\boldsymbol{H}$.

1) Increasing all Ω_i is the most trivial approach. In fact, $\boldsymbol{H}$ is retained by driving $\boldsymbol{H}$ away from the origin by the RW effect and counterdrive by the CMG subsystem. The impassable surface moves to B from the original one (A in Fig. 9b).

2) The previous SR inverse method makes lateral $\boldsymbol{H}$ motion of the CMG subsystem and a counter-RW effect makes the impassable surface move to C or D in Fig. 9b.

3) The singular surface around point V is type 2 and $1/\kappa$ is negative. Because p_4 is the only negative term to make $1/\kappa$ in Eq. (9) negative, reducing Ω_4 is effective to reduce the absolute value of $1/\kappa$ as F in Fig. 9b. Without motion by the CMG subsystem and without RW torque, the impassable surface can be changed more, as G in Fig. 9b.

Although the latter two approaches, especially their combination, shown as I in Fig. 9b, seem to be more effective than the first, it remains unclear how the proposed methods manage to combine them. Because the total system has more degrees of freedom than the CMG subsystem, an additional measure to usual singularity measure might be necessary for a proper gradient method.

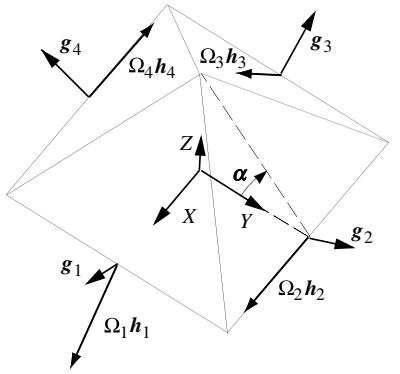

a) Impassable singular state

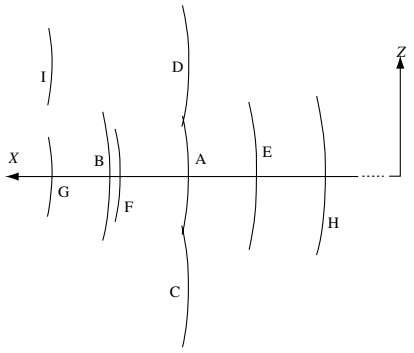

b) Change of impassable surface

Fig. 9 Change of impassable surface by VSCMG. a) σ: $(-1/2\pi, \pi, 1/2\pi, \pi)$. b) Cross sections by x–z plane of the impassable singular surfaces near point V in Fig. 2b are drawn with various Ω_i. The RW term, Ω_i, is changed as the following: A—(1, 1, 1, 1), B—(1.05, 1.05, 1.05, 1.05), C—(0.95, 1, 1.05, 1), D—(1.05, 1, 0.95, 1), E—(1, 1, 1, 1.05), F—(1, 1, 1, 0.95), G—(1, 1.05, 1, 0.95), H—(1, 0.95, 1, 1.05), I—(1.05, 1.05, 0.95, 0.95). Although another impassable surface exists in this area and it also changes, the singular state σ corresponding to this surface is distant from the current state; for that reason, it is not drawn.

E. Maneuvering

In many papers, a certain maneuvering task using the pyramid-type system is used mostly for simulations; it requires an $\boldsymbol{H}$ path from the origin along the x axis passing through point V in Fig. 2b [6–9]. Because the impassable surface near V (E or W) is the narrowest along the surface strip, the expected error of $\boldsymbol{H}$ is smaller than that by other maneuvering commands, for example, passing through M in Fig. 2a.

The analysis presented in Sec. V.B subsumes that the command torque is constant. This is assured in usual maneuvering with large satellite's moment of inertia because a satellite's rotation is sufficiently small when $\boldsymbol{H}$ reaches its maximum. If $\boldsymbol{H}$ is trapped at an internal impassable surface, however, the satellite's rotation cannot be neglected and the torque command will be changed. In this case, sliding by the change of the torque command cannot be neglected. Therefore, a dynamics simulation alone is insufficient for evaluation of a steering law.

As described in Sec V.B, errors of $\boldsymbol{H}$ by the SR inverse-type steering laws are similar, but there are differences in torque error. If we consider a simple dynamics model of one axis rotation with the same maximum error of $\boldsymbol{H}$, the final attitude error is minimized by control with the maximum torque error, not the minimum, and therefore with the shortest duration. Although three-axis rotation dynamics are not simple, torque error is less important than $\boldsymbol{H}$ error. Actually, the experimental comparison provided in [38] shows few significant differences among various steering laws with regard to the sliding motion.

For maneuvering, $\boldsymbol{H}$ deviates, seemingly unavoidably, by all the SR inverse-type steering laws for specific commands. The deviation of $\boldsymbol{H}$ can resemble that by offline reshaping described in Sec. IV.B. Because the offline reshaping is exceedingly simple, it can be a

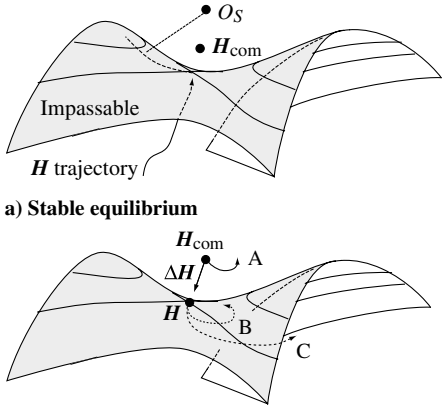

Fig. 10 Pointing control near impassable singular state. O_S: center of principal curvature of the surface. A: trajectory of the target H_{com} attributable to the satellite's motion. B and C: trajectory of H.

competitive method for the symmetric pyramid-type CMG system for maneuvering.

F. Pointing and Tracking

Few papers have described pointing or tracking control of a satellite using a CMG system. Among the exceptions, [39] does not address singularity avoidance, [40] does not describe details, and [41,42] present analyses of VSCMGs. Using a simplified example, we examine a problem of a pointing task using a typical CMG system controlled by an SR inverse-type steering law [28].

Suppose a situation in which the attitude of the satellite is maintained under disturbance torque. Because a precise pointing is retained, the CMG system fully accumulates the angular momentum by the disturbance torque. In this situation, it is understood that the vector $\boldsymbol{H}$ of the CMG system is controlled to track a command vector $\boldsymbol{H}_{com}$, which is a time integral of the disturbance torque in the CMG coordinate. Further assuming that the disturbance torque is sufficiently small and almost constant, this tracking control as well as singularity avoidance by a gradient method works well if the CMG system is far from a singular state. If $\boldsymbol{H}_{com}$ moves through an impassable surface, as shown in Fig. 10a, and if the CMG state is near the impassable singular state, however, tracking control cannot be maintained. Because $\boldsymbol{H}_{com}$ is near the surface immediately after it crosses the surface, nearer than the center of the principal curvature of the surface, the sliding effect by the SR inverse-type steering laws described in the preceding section will not work and $\boldsymbol{H}$ will stay as a stable equilibrium.

Once tracking of $\boldsymbol{H}$ to $\boldsymbol{H}_{com}$ fails, the satellite's attitude cannot be maintained; we must consider the satellite's subsequent motion. The satellite rotates with angular momentum of the error term, $\boldsymbol{H}_{com} - \boldsymbol{H}$; subsequently, $\boldsymbol{H}_{com}$ moves in the CMG coordinate and $\boldsymbol{H}$ follows it by sliding, as in Fig. 10b. The satellite's rotation depends on the accumulated angular momentum and asymmetry of the satellite's inertial moments. If this motion is small, $\boldsymbol{H}$ remains on the singular surface (B in Fig. 10b); if it is large, $\boldsymbol{H}$ escapes from the surface (C in Fig. 10b). Nevertheless, a large angular error and/or long duration are inevitable, even though the error, $\boldsymbol{H}_{com} - \boldsymbol{H}$, is small.

Therefore, along with the SR inverse-type steering laws, no exact type steering law is able to overcome this problem. If another means of torque generation is available, such as that by RW effect of VSCMGs or by an unloading torquer, escape from this situation is possible without causing attitude error. Otherwise, active change of $\boldsymbol{H}$ overlooking transient attitude error is necessary, similarly as that proposed in [32,34].

VI. Conclusions

A geometrical theory of CMG singular surface and steering laws, especially of their singularity avoidance methods, were surveyed. The theory has become fruitful by virtue of many researchers' efforts, and is sufficient for selection and evaluation of configurations as well as for analysis of steering laws. For steering law and singularity avoidance, sufficiently various means have been tried: gradient methods for appropriate system configurations, offline planning and workspace restriction for exact steering, allowance of error in output torque, and the use of other degrees of freedom, with VSCMGs or with unloading torquers. No perfect steering law exists, especially for the pyramid-type system.

Selection of a steering law depends on mission requirements. For celestial observations, for example, long-duration precise pointing is required for high-resolution image acquisition, tracking is required for mapping, and rapid maneuvering is required for observation of scattered celestial objects. In any case, pointing performance cannot be neglected, but too few studies have been undertaken to study pointing and tracking.

The required shape of the $\boldsymbol{H}$ workspace, that is, the envelope, also depends on the mission requirements, expected disturbance profile, and maneuvering method. The pyramid type was selected in most studies mainly because its envelope resembles a sphere. A satellite's moment of inertia and the profile of the disturbance, however, are anisotropic in most cases. Therefore, a near spherical envelope is not always optimal. The roof-type system was eliminated from consideration not because of its envelope shape but because the pyramid-type system was a superior candidate, even with its unclear problems. Now that it is established that no perfect steering law exists for the pyramid-type system, the roof-type system can be reconsidered as a candidate.

Moreover, it is worthwhile to reexamine several research issues that have been studied, with the backdrop of advanced space technology. Some issues that are not discussed in this paper are the feasible number of CMG units, the installation direction of a CMG system to a satellite, and the merits and demerits of gimbal limits.

Appendix: Mathematical Details and Conjectures

Infinitesimal displacement of $\boldsymbol{H}$, $\Delta\boldsymbol{H}$, by $d\sigma$ is described using a Taylor series as

$$\Delta\boldsymbol{H} = \boldsymbol{H}(\sigma^S + d\sigma) - \boldsymbol{H}(\sigma^S) = \boldsymbol{C}d\sigma + 1/2\sum d\boldsymbol{c}_i^S d\sigma_i + O(|d\sigma|^3)$$

$$= \boldsymbol{C}d\sigma - 1/2\sum \boldsymbol{h}_i^S d\sigma_i^2 + O(|d\sigma|^3) \tag{A1}$$

Taking the inner product with $\boldsymbol{u}$ and ignoring higher-order terms, expression in Eq. (14) is obtained.

The motion by $d\sigma^S$ keeps the system singular; thereby, Eq. (5) is retained. The differential of Eq. (5) leads to

$$d\boldsymbol{u}\cdot\boldsymbol{c}_i^S = -\boldsymbol{u}\cdot d\boldsymbol{c}_i^S = \boldsymbol{u}\cdot(\boldsymbol{h}_i^S d\sigma_i^S) = q_i d\sigma_i^S \tag{A2}$$

where $d\boldsymbol{u}$ is $d\boldsymbol{u}(d\sigma^S)$. By that relation,

$$\sum q_i d\sigma_i^N d\sigma_i^S = \sum d\sigma_i^N (d\boldsymbol{u}\cdot\boldsymbol{c}_i^S) = d\boldsymbol{u}\cdot\sum \boldsymbol{c}_i^S d\sigma_i^N = 0 \tag{A3}$$

This leads to Eq. (22). Using Eq. (A2), we obtain

$$Q(d\sigma^S) = \sum q_i (d\sigma_i^S)^2 = \sum (d\boldsymbol{u}\cdot\boldsymbol{c}_i^S) d\sigma_i^S = d\boldsymbol{u}\cdot d\boldsymbol{H}(d\sigma^S) \tag{A4}$$

This is the definition of the second fundamental form of the surface.

Surface regularity implies that the second fundamental form is not 0, that is, $d\boldsymbol{H}(d\sigma^S) = \mathrm{Q}(d\sigma^S) \neq 0$, for $d\boldsymbol{u}$ and $d\boldsymbol{H}$ along both principal directions. Where the regularity breaks, there are three cases in which $d\boldsymbol{u}$ is along one principal direction: 1) $d\boldsymbol{u} = d\boldsymbol{H} = 0$, 2) $d\boldsymbol{u} \neq 0$ and $d\boldsymbol{H} = 0$, 3) $d\boldsymbol{u} = 0$ and $d\boldsymbol{H} \neq 0$. For an independent-type configuration, $d\boldsymbol{u} \neq 0$ for any $d\sigma^S$ because of Eq. (A2), which suggests that, although they have not been proven, such states are not degenerate. For a multiparallel configuration, all three cases are possible; degenerate states have been found as of the first two cases. Unproved mathematical conjectures including this are listed as follows. Their proofs and counterproofs remain as subjects for future study.

Conjecture 1: There is no degenerate state for any independent-type configuration.

Conjecture 2: $\boldsymbol{H} \cdot \boldsymbol{u} > 0$, that is, the vector $\boldsymbol{u}$ is directed outward at an impassable surface.

Conjecture 3: The range of $\boldsymbol{H}$ is simply connected for any system configuration.

Conjecture 3 is automatically proved if conjecture 2 is true.

Acknowledgments

The author thanks Nobuyuki Yajima, a former professor of the Institute of Space and Astronautical Science, and Shigeru Kokaji, the former Deputy Director of the Systems Science Research Institute of the National Institute of Advanced Industrial Science and Technology, for sustained support and intensive discussions.

References

[1] NASA Marshall Space Flight Center, "A Comparison of CMG Steering Laws for High Energy Astronomy Observatories (HEAOs)," NASA TM X-64727, 1972.

[2] Yoshikawa, T., "A Steering Law for Three Double Gimbal Control Moment Gyro System," NASA TM-X-64926, 1975.

[3] Cornick, D. E., "Singularity Avoidance Control Laws for Single Gimbal Control Moment Gyros," AIAA Paper 79-1698, 1979, pp. 20–33.

[4] Hefner, R. D., and McKenzie, C. H., "A Technique for Maximizing the Torque Capability of Control Moment Gyro Systems," *Astrodynamics*, Vol. 54, No. AAS 83-387, 1983, pp. 905–920.

[5] Bedrossian, N. S., Paradiso, J., Bergmann, E. V., and Rowell, D., "Steering Law Design for Redundant Single-Gimbal Control Moment Gyroscope," *Journal of Guidance, Control, and Dynamics*, Vol. 13, No. 6, 1990, pp. 1083–1089.

[6] Oh, H., and Vadali, S., "Feedback Control and Steering Laws for Spacecraft Using Single Gimbal Control Moment Gyro," *Journal of the Astronautical Sciences*, Vol. 39, No. 2, 1991, pp. 183–203.

[7] Ford, K. A., and Hall, C. D., "Singular Direction Avoidance Steering for Control Moment Gyros," *Journal of Guidance, Control, and Dynamics*, Vol. 23, No. 4, 2000, pp. 648–656.

[8] Wie, B., Bailey, D., and Heiberg, C. J., "Singularity Robust Steering Logic for Redundant Single-Gimbal Control Moment Gyros," *Journal of Guidance, Control, and Dynamics*, Vol. 24, No. 5, 2001, pp. 865–872.

[9] Wie, B., "New Singularity Escape and Avoidance Steering Logic for Control Moment Gyro Systems," AIAA Paper 2003-5659, 2003, pp. 2191–2201.

[10] NASA Langley Research Center, "Integrated Power/Attitude Control System (IPACS)," NASA CP-2290, 1983.

[11] Schaub, H., Vadali, S. R., and Junkins, J. L., "Feedback Control Law for Variable Speed Control Moment Gyroscopes," *Journal of the Astronautical Sciences*, Vol. 46, No. 3, 1998, pp. 307–328.

[12] Schaub, H., and Junkins, J. L., "Singularity Avoidance Using Null Motion and Variable-Speed Control Moment Gyros," *Journal of Guidance, Control, and Dynamics*, Vol. 23, No. 1, 2000, pp. 11–16.

[13] Yoon, H., and Tsiotras, P., "Spacecraft Adaptive Attitude and Power Tracking with Variable Speed Control Moment Gyroscopes," *Journal of Guidance, Control, and Dynamics*, Vol. 25, No. 6, 2002, pp. 1081–1090.

[14] Yoon, H., and Tsiotras, P., "Singularity Analysis of Variable Speed Control Moment Gyros," *Journal of Guidance, Control, and Dynamics*, Vol. 27, No. 3, 2004, pp. 374–386.

[15] Yoon, H., and Tsiotras, P., "Spacecraft Line-of-Sight Control Using a Single Variable-Speed Control Moment Gyro," *Journal of Guidance, Control, and Dynamics*, Vol. 29, No. 6, 2006, pp. 1295–1308.

[16] Margulies, G., and Aubrun, J. N., "Geometric Theory of Single-Gimbal Control Moment Gyro System," *Journal of the Astronautical Sciences*, Vol. 26, No. 2, 1978, pp. 159–191.

[17] Tokar, E. N., "Efficient Design of Powered Gyrostabilizer Systems," *Cosmic Research*, 1978, pp. 16–23; also *Kosmicheskie Issledovaniya*, Vol. 16, No. 1, 1978, pp. 22–30.

[18] Tokar, E. N., "Problems of Gyroscopic Stabilizer Control," *Cosmic Research*, 1978, pp. 141–147; also *Kosmicheskie Issledovaniya*, Vol. 16, No. 2, 1978, pp. 179–187.

[19] Tokar, E. N., "Effect of Limiting Supports on Gyro Stabilizer," *Cosmic Research*, 1979, pp. 413–420; also *Kosmicheskie Issledovaniya*, Vol. 16, No. 4, 1978, pp. 505–513.

[20] Tokar, E. N., and Platonov, V. N., "Singular Surfaces in Unsupported Gyrodyne Systems," *Cosmic Research*, 1979, pp. 547–555; also *Kosmicheskie Issledovaniya*, Vol. 16, No. 5, 1978, pp. 675–685.

[21] Kurokawa, H., Yajima, N., and Usui, S., "A New Steering Law of a Single-Gimbal CMG System of Pyramid Configuration," *Proceedings of IFAC Automatic Control in Space*, Pergamon, Oxford, England, U.K., 1985, pp. 251–257.

[22] Kurokawa, H., and Yajima, N., "A Study of Single Gimbal CMG System," *Proceedings of 15th International Symposium on Space Technology and Science (ISTS)*, AGNE Publishing, Inc., Tokyo, Japan, 1986, pp. 1219–1224.

[23] Kurokawa, H., "A Study of CMG Systems-for Selection and Evaluation," *Proceedings of 16th International Symposium on Space Technology and Science (ISTS)*, AGNE Publishing, Inc., Tokyo, Japan, 1988, pp. 1243–1249.

[24] Bedrossian, N. S., Paradiso, J., and Bergmann, E. V., "Redundant Single Gimbal Control Moment Gyroscope Singularity Analysis," *Journal of Guidance, Control, and Dynamics*, Vol. 13, No. 6, 1990, pp. 1096–1101.

[25] Kurokawa, H., "Exact Singularity Avoidance Control of the Pyramid Type CMG System," AIAA Paper 94-3559-CP, 1994, pp. 170–180.

[26] Wie, B., "Singularity Analysis and Visualization for Single-Gimbal Control Moment Gyro Systems," *Journal of Guidance, Control, and Dynamics*, Vol. 27, No. 2, 2004, pp. 271–282.

[27] Kurokawa, H., "Geometrical View to Steering of the Pyramid Type CMG System," *Proceedings of 18th International Symposium on Space Technology and Science (ISTS)*, AGNE Publishing, Inc., Tokyo, Japan, 1992, pp. 1051–1057.

[28] Kurokawa, H., "A Geometric Study of Single Gimbal Control Moment Gyros-Singularity and Steering Law," Ph.D. Dissertation, Aeronautics and Astronautics, Univ. Tokyo, Tokyo, 1997; Report of Mechanical Engineering Laboratory, No. 175, 1998, http://staff.aist.go.jp/kurokawa-h/CMGpaper97.pdf.

[29] Gottlieb, D. H., "Robots and Topology," *Proceedings of IEEE International Conference on Robotics and Automation*, IEEE, Piscataway, NJ, 1986, pp. 1689–1691.

[30] Bauer, S. R., "Difficulties Encountered In Steering Single Gimbal CMGs," The Charles Stark Draper Laboratory, Inc., Space Guidance and Navigation Memo No. 10E-87-09, 1987.

[31] Crenshaw, J. W., "2-Speed, a Single Gimbal CMG Attitude Control System," Northrop Services Inc., TR-243-1139 (NASA CR), 1972.

[32] Yoshikawa, T., "Steering Law for Roof Type Configuration Control Moment Gyro System," *Automatica*, Vol. 13, 1979, pp. 359–368.

[33] Vadali, S. R., Oh, H. S., and Walker, S. R., "Preferred Gimbal Angles for Single Gimbal Control Moment Gyros," *Journal of Guidance, Control, and Dynamics*, Vol. 13, No. 6, 1990, pp. 1090–1095.

[34] Kurokawa, H., "Constrained Steering Law of Pyramid-Type Control Moment Gyros and Ground Tests," *Journal of Guidance, Control, and Dynamics*, Vol. 20, No. 3, 1997, pp. 445–449.

[35] Paradiso, J., "Global Steering of Single Gimballed Control Moment Gyroscopes Using a Directed Search," *Journal of Guidance, Control, and Dynamics*, Vol. 15, No. 5, 1992, pp. 1236–1244.

[36] Defendini, A., Lagadec, K., Guay, P., and Griseri, G., "Low Cost CMG-Based AOCS Designs," *Proceedings of the 4th ESA International Conference Spacecraft Guidance, Navigation and Control Systems*, ESA Publishing Division, ESTEC, Noordwijk, The Netherlands, 1999, pp. 393–398.

[37] Nakamura, Y., and Hanafusa, H., "Inverse Kinematic Solutions with Singularity Robustness for Robot Manipulator Control," *Journal of Dynamic Systems, Measurement, and Control*, Vol. 108, No. 3, 1986, pp. 163–171.

[38] Jung, D., and Tsiotras, P., "An Experimental Comparison of CMG Steering Control Laws," AIAA Paper 2004-5294, 2004, pp. 1128–1144.

[39] Heiberg, C. J., Bailey, D., and Wie, B., "Precision Spacecraft Pointing Using Single-Gimbal Control Moment Gyroscopes with Disturbance," *Journal of Guidance, Control, and Dynamics*, Vol. 23, No. 1, 2000, pp. 77–85.

[40] Wie, B., Bailey, D., and Heiberg, C., "Rapid Multitarget Acquisition and Pointing Control of Agile Spacecraft," *Journal of Guidance, Control, and Dynamics*, Vol. 25, No. 1, 2002, pp. 96–104.

[41] Marshall, A., and Tsiotras, P., "Spacecraft Angular Velocity Stabilization Using a Single-Gimbal Variable Speed Control Moment Gyro," AIAA Paper 2003-5654, 2003, pp. 11–14.

[42] Yoon, H., and Tsiotras, P., "Spacecraft Angular Velocity and Line-of-Sight Control Using A Single-Gimbal Variable-Speed Control Moment Gyro," AIAA Paper 2005-6393, 2005, pp. 15–18.